

# THE MOTION OF CHARGED PARTICLES IN THE VICINITY OF MAGNETIC NEUTRAL PLANES WITH APPLICATIONS TO TYPE III SOLAR RADIO BURSTS

By A. A. WEISS\* and J. P. WILD\*

[Manuscript received December 18, 1963]

## Summary

The equations of motion for a charged particle of constant energy injected into or near a neutral plane separating two opposing magnetic fields are integrated by approximate analytical methods. The simplest relevant field configuration, with an arbitrary intensity gradient in one direction, is chosen. The trajectories of particles injected at arbitrary angles and at points in or near to the neutral plane are discussed in detail.

The motions of the guiding centres and the spatial density distributions of clouds of particles are evaluated for the exponential model, in which the vertical field intensity decreases exponentially in the vertical direction. When clouds of particles are discussed, mutual interactions of the particles are neglected, as are interactions between the particles and any background plasma that may be supposed to exist. On the supposition that the sources of type III solar radio bursts are compact clouds of electrons guided by magnetic neutral planes in the solar corona, the exponential model is discussed as a possible model for type III bursts. Observed features of type III bursts are found to be consistent with the model.

## I. INTRODUCTION

In this paper we study the motion of charged particles injected into or near a neutral plane separating two opposing magnetic fields whose intensity varies monotonically in a specified direction along the neutral plane. We shall show that the particles are guided and gyrated by the field configuration, in a manner somewhat analogous to, but more complex than, the case in which a finite magnetic field increases along the direction of the lines of force (culminating in the well-known "magnetic mirror").

Apart from its intrinsic interest, the neutral plane problem is relevant to solar physics, particularly in respect of flares and their radio accompaniments. Optical evidence (admittedly controversial) has been reported that flares may occur at the conjunction of strong opposing magnetic fields (e.g. Severny 1962), and electromagnetic theories of flares (Dungey 1958; Sweet 1958; Gold and Hoyle 1959) envisage that the flare energy is released near neutral points or planes by the partial destruction of opposing sunspot fields.† The expansion and approach of opposing bipolar magnetic regions (Babcock 1962) may also generate neutral planes, extending to great heights in the corona, along which the compact clouds of electrons held responsible for solar radio bursts of type III are able to move freely.

\* Division of Radiophysics, CSIRO, University Grounds, Chippendale, N.S.W.

† The theoretical difficulties associated with the magnetic theories of flares have recently been examined by Parker (1963). These difficulties might be overcome by the recent theory of Petschek (1963).

II. GENERAL EQUATIONS FOR A SINGLE CHARGED PARTICLE

(a) *The Basic Equations*

For the magnetic field we adopt the simple configuration, in a rectangular coordinate system,

$$\left. \begin{aligned} B_x &= -\frac{1}{2}x^2 \frac{db(z)}{dz}, \\ B_y &= 0, \\ B_z &= xb(z). \end{aligned} \right\} \quad (1)$$

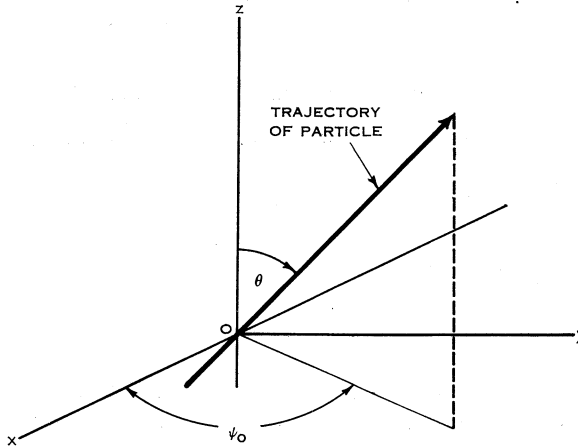


Fig. 1.—Illustrating the system of angular variables. *Oyz* is the neutral plane. The azimuth angle  $\psi_0$  is the angle in the *x-y* plane at which the particle crosses the neutral plane. The pitch angle  $\theta$  is a function of the magnetic field gradient in the direction *Oz*.

The *Oyz* plane is the neutral ( $B = 0$ ) plane (Fig. 1); we shall refer to the *z*-direction as the “vertical”. The vertical field gradient,  $b(z)$ , is a slowly varying function of *z*. The field configuration thus defined appears to be the simplest relevant one satisfying the condition  $\text{div } \mathbf{B} = 0$ .

In the absence of collisions or mechanisms (e.g. electric fields) which alter the kinetic energy,\* the equations of motion of a charged particle in the field specified by (1) are

$$m \frac{d^2x}{dt^2} = \frac{eb}{c} x \frac{dy}{dt}, \quad (2a)$$

$$m \frac{d^2y}{dt^2} = -\frac{e}{c} \left( x^2 \frac{db}{dz} \frac{dz}{dt} + bx \frac{dx}{dt} \right) = -\frac{e}{2c} \frac{d}{dt} (bx^2), \quad (2b)$$

$$m \frac{d^2z}{dt^2} = \frac{e}{2c} x^2 \frac{db}{dz} \frac{dy}{dt}, \quad (2c)$$

\* We confine our treatment to non-relativistic motion.

where  $e$  and  $m$  are respectively the charge and mass of the particle and  $c$  is the velocity of light. In this and the next section we consider only particles actually injected into the neutral plane. For such particles the equations (2) describe a motion comprising drift velocities in the  $y$ - and  $z$ -directions, superimposed on periodic oscillatory motion in all three dimensions. We have been unable to obtain exact solutions to these equations and an approximate solution in terms of elliptic integrals is given below. Analytic expressions are obtained for the drift motion in the  $y$ - $z$  plane, and for the oscillatory motions in the  $x$ - $y$  plane. The effect of the method of solution, as a first approximation, is to average out the oscillatory motion in the  $y$ - $z$  plane; if desired, the periodic part of the motion in the  $y$ - $z$  plane could be recovered by a second-order approximation.

(b) *The Motion in the  $z$ -direction*

To determine the vertical drift motion  $v_z$  we first rewrite (2c) as

$$v_z \frac{dv_z}{db} = \frac{e}{2mc} x^2 v_y, \quad (3)$$

and integrate (2b) to obtain

$$v_y = -\frac{eb}{2mc} x^2 + v_1 \sin \psi_0, \quad (4)$$

where  $v_1$  denotes the transverse velocity  $(v_x^2 + v_y^2)^{\frac{1}{2}}$ , and  $\psi_0$  is the angle in the  $x$ - $y$  plane at which the trajectory of the particle crosses the neutral plane (Fig. 1).

The value of  $x^2 v_y$  in equation (3) varies greatly over a single loop, but varies only slowly from loop to loop as  $b$  varies with  $z$ . We therefore integrate (3) using not the instantaneous value but the mean value of  $\langle x^2 v_y \rangle_{b(z)}$  over a loop, calculated on the assumption that  $b(z)$  can be regarded as constant throughout one loop. With this assumption,  $\psi_0$  is an invariant of the motion.  $\langle x^2 v_y \rangle_{b(z)}$  is evaluated in Appendix I; we find

$$\langle x^2 v_y \rangle_{b(z)} = -\frac{mc}{e} \frac{\gamma(\psi_0) v_1^2}{b(z)}, \quad (5)$$

in which

$$\gamma(\psi_0) = \frac{2}{3} \{1 + (2E/K - 1) \sin \psi_0\}. \quad (6)$$

$E$  and  $K$  are the complete elliptic integrals of modulus

$$\lambda = \frac{1}{2} \psi_0 + \frac{1}{4} \pi.$$

The parameter  $\gamma$  is sketched in Figure 2.

Since  $(v_1^2 + v_z^2)^{\frac{1}{2}} = V$ , the total (constant) speed of the particle, and  $\gamma$  is independent of  $z$ , integration of (3) with (5) gives for the vertical component of the drift motion (whose direction is independent of the sign of the charge)

$$v_z = V[1 - \{b/b(0)\} \gamma \sin^2 \theta_0]^{\frac{1}{2}}. \quad (7)$$

Here  $\theta$  is the pitch angle (inclination of the trajectory to the  $z$ -axis, Fig. 1). Thus

$$\sin^2 \theta / \sin^2 \theta_0 = [b/b(0)] \gamma. \quad (8a)$$

Since  $\gamma < 1$ , the rate of decrease of pitch angle with decreasing field intensity parallel to the neutral plane is less than the corresponding decrease in pitch angle for a particle spiralling round a line of force in a simple configuration free of neutral planes, for which we have the well-known formula

$$\sin^2\theta/\sin^2\theta_0 = B/B_0. \tag{8b}$$

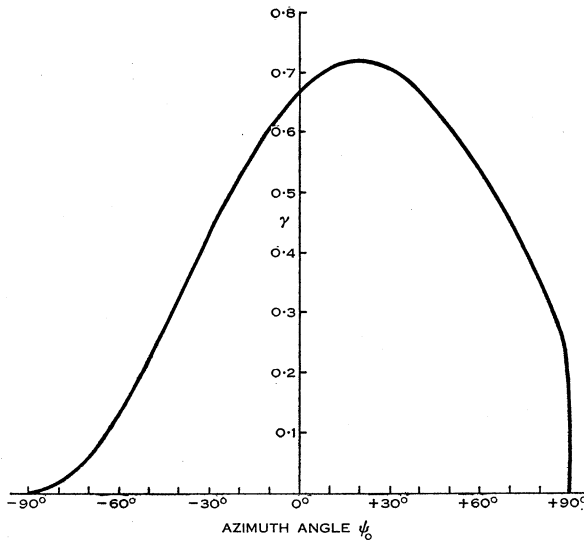


Fig. 2.—The parameter  $\gamma$  (equation (6); evaluated in Appendix I) as a function of the injection azimuth angle  $\psi_0$ .

(c) Motion in the x-y Plane\*

Retaining the assumption of the constancy of  $b(z)$  over a single loop, the integral of (2a) is

$$v_x^2 = v_{\perp}^2 \cos^2\psi_0 + C(z)x^2 v_{\perp} \sin\psi_0 - \frac{1}{4}\{C(z)\}^2 x^4,$$

where

$$C(z) = eb(z)/mc.$$

Hence we see that there is no continuous drift motion in the  $x$ -direction; in fact, the  $x$ -motion is confined within the limits

$$x_{lim} = \pm 2(v_{\perp}/C)^{\frac{1}{2}} \sin\lambda. \tag{9}$$

In order to obtain the trajectories in the  $x$ - $y$  plane we return to equation (4) for  $v_y$ . Recalling that  $v_x^2 = v_{\perp}^2 - v_y^2$ , and using the substitution

$$\cos\phi = \frac{1}{2}(C/v_{\perp})^{\frac{1}{2}}(x/\sin\lambda) = x/x_{lim}, \tag{10}$$

we obtain

$$dy/d\phi = (v_{\perp}/C)^{\frac{1}{2}}\{2(1 - \sin^2\lambda \sin^2\phi)^{\frac{1}{2}} - (1 - \sin^2\lambda \sin^2\phi)^{-\frac{1}{2}}\}.$$

\* The results of this section have already been given by Seymour (1959).

Taking  $t = 0$  when  $x = 0$  and  $y = 0$ , the last expression integrates to give

$$y = Y - (v_{\perp}/C)^{\frac{1}{2}}\{F(\phi, \lambda) - 2E(\phi, \lambda)\}, \tag{11}$$

where  $F(\phi, \lambda)$  and  $E(\phi, \lambda)$  are the incomplete elliptic integrals of the first and second kinds, and  $Y$  is the total displacement in the  $y$ -direction over a quarter-loop, given by

$$Y = (v_{\perp}/C)^{\frac{1}{2}}\{K - 2E\}. \tag{12}$$

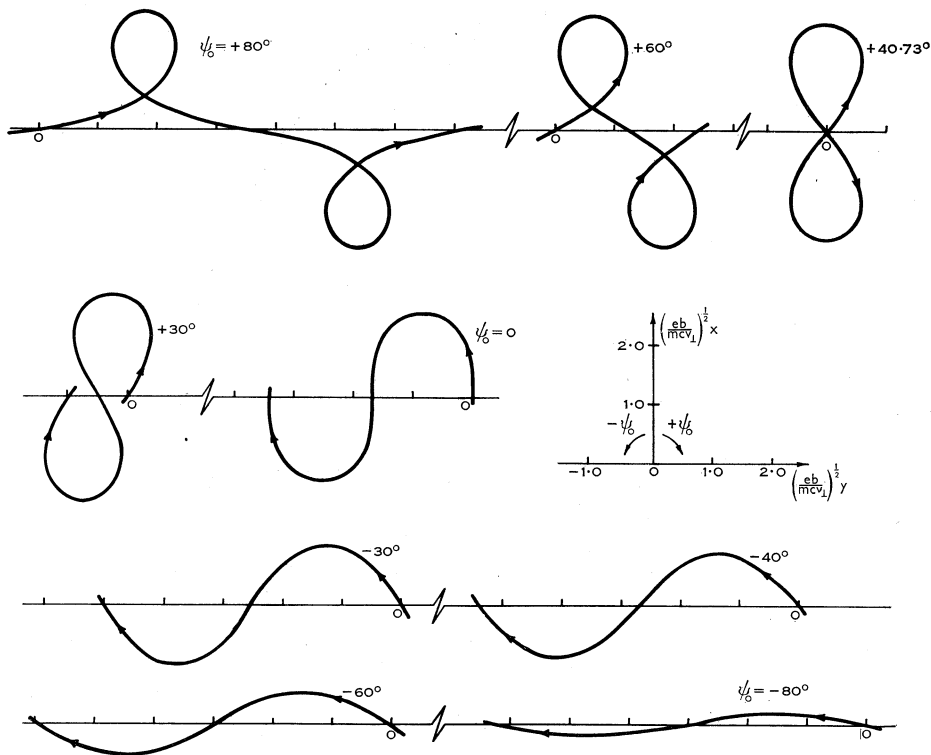


Fig. 3.—Trajectories in the  $x$ - $y$  plane. In each case the particle is injected at  $O$  with the azimuth angle  $\psi_0$  indicated against the trajectory, and moves in the direction shown by the arrow. For  $\psi_0 = +40.73^\circ$  (when  $2E = K$ , argument  $\frac{1}{2}\psi_0 + \frac{1}{4}\pi$ ) the guiding centre moves vertically up the  $z$ -axis. The unit of length is  $\{eb(z)/mcv_{\perp}\}^{\frac{1}{2}}$ , which is assumed to be constant over the loop.

Equations (10) and (11) are parametric equations for the loops in the  $x$ - $y$  plane. The loops for several values of  $\psi_0$  are drawn in Figure 3.

For the time elapsed since the passage of the particle through the origin we have

$$\begin{aligned} dt/d\phi &= (Cv_{\perp})^{-\frac{1}{2}}(1 - \sin^2\lambda \sin^2\phi)^{-\frac{1}{2}}, \\ t &= T - (Cv_{\perp})^{-\frac{1}{2}}F(\phi, \lambda), \end{aligned} \tag{13}$$

where  $T$ , the total time for a quarter-loop, is simply

$$T = (Cv_{\perp})^{-\frac{1}{2}}K. \tag{14}$$

The depth of penetration of the magnetic field by the particle depends on the field intensity; it may be written in terms of an equivalent "gyro radius". From (1) and (9),

$$x_{\text{lim}} = \frac{v_{\perp} mc}{eB_{z,\text{lim}}} \{2(1 + \sin \psi_0)\},$$

where  $B_{z,\text{lim}}$  is the  $z$ -component of the field intensity at  $x_{\text{lim}}$ . But  $v_{\perp} mc/eB_{z,\text{lim}} = a$ , the radius of gyration of a particle in the constant field  $B_{z,\text{lim}}$ , and hence the equivalent gyro radius of the loop is  $2a(1 + \sin \psi_0) \leq 4a$ . In the same way we derive an equivalent "gyro frequency"

$$f = (\pi^2/4K^2)f_B,$$

where  $f_B = eB_{z,\text{lim}}/2\pi mc$  is the gyro frequency for constant field  $B_{z,\text{lim}}$ . Over most of the range of  $\psi_0$ ,  $f \sim f_B$ , but  $f \rightarrow 0$  as  $\psi_0 \rightarrow \frac{1}{2}\pi$ .

Finally, the mean drift rate in the  $y$ -direction may be obtained from (12) and (14), thus

$$\bar{v}_y = v_{\perp}(1 - 2E/K). \quad (15)$$

#### (d) Motion of the Guiding Centre

The guiding centre follows a trajectory in the neutral ( $y$ - $z$ ) plane with the average drift motions given by (7) and (15), and the oscillatory motions in all three dimensions take place about this guiding centre. Writing in the magnetic field gradient explicitly, the equations of motion of the guiding centre are expressed in terms of the injection parameters  $V$ ,  $\theta_0$ ,  $\psi_0$ , and  $\gamma(\psi_0)$  as:

$$x = 0,$$

$$dy/dt = V\{(1 - 3\gamma/2)/\sin \psi_0\}\{b/b(0)\}^{\frac{1}{2}\gamma} \sin \theta_0, \quad (16a)$$

$$dz/dt = V[1 - \{b/b(0)\}^{\gamma} \sin^2 \theta_0]^{\frac{1}{2}}. \quad (16b)$$

If  $b(z)$  decreases monotonically to small values as  $z$  increases, the trajectories of the guiding centres eventually become vertical, whatever the injection conditions (except for particles injected directly along the neutral plane, when  $\psi_0 = \pm \frac{1}{2}\pi$ ), and at large heights above the point of injection into the neutral plane the particles travel vertically with their injection speed  $V$ . The shapes of the trajectories of the guiding centres, and the times required for the achievement of essentially vertical rectilinear motion, are independent of the absolute magnetic field intensity, but depend on the field configuration. It should be noted (see equation (6)) that  $\gamma$  is not symmetrical about  $\psi_0 = 0$ , and hence the guiding centres are not disposed symmetrically about the  $z$ -axis.

#### (e) Special Case of an Exponential Field Variation

More detailed consideration of the motions of the guiding centres requires specification of the vertical field gradient function  $b(z)$ . We now explore the trajectories generated in a simple field configuration which has the advantage that the equations of motion (16) can be integrated analytically. In this configuration, which

we term the exponential model, the vertical field strength decreases exponentially with increasing height, that is,

$$b(z) = b(0)e^{-kz}.$$

Integrating (16a) and (16b), we obtain the parametric equations for the trajectory of the guiding centre for a single particle in the  $y$ - $z$  plane:

$$y = -(4/k \sin \psi_0)(3/2 - 1/\gamma)\{\arctan(e^{1/2\gamma k V t} \cot \frac{1}{2}\theta_0) - \frac{1}{2}(\pi - \theta_0)\}, \tag{17a}$$

$$z = (2/k\gamma)\ln[\sin \theta_0 \cosh\{\frac{1}{2}\gamma k V t - \ln \tan(\frac{1}{2}\theta_0)\}]. \tag{17b}$$

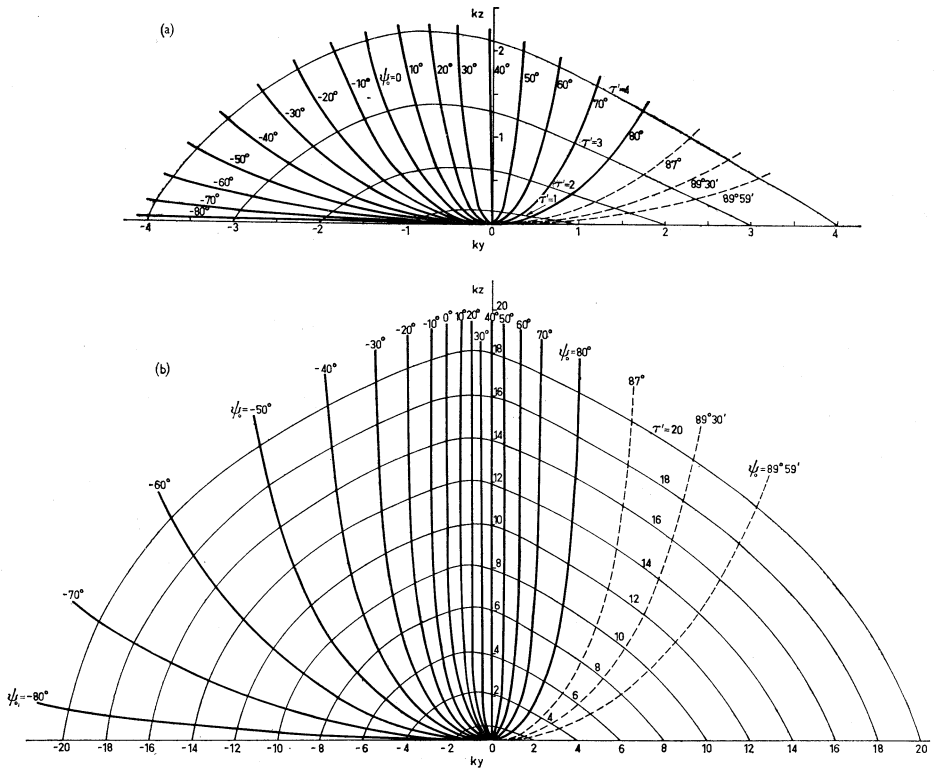


Fig. 4.—Trajectories and constant-time lines in the neutral plane for the guiding centres of particles injected in an exponential ( $b = b(0)e^{-kz}$ ) model with pitch angle  $\theta_0 = \frac{1}{2}\pi$ . Each trajectory is labelled with the value of  $\psi_0$ , the angle in the  $x$ - $y$  plane at which the particle crosses the neutral plane. Constant-time lines are labelled with  $\tau' = kVt$ . Part (a) is an enlargement ( $\times 4$ ), in the vicinity of the injection point, of part (b).

Trajectories and constant-time lines are plotted in Figure 4 for the case of horizontal injection into the neutral plane,  $\theta_0 = \frac{1}{2}\pi$ . This diagram illustrates the achievement of essentially rectilinear vertical motion at not too large values of  $kVt$  (provided  $\psi_0$  does not approach  $\pm\frac{1}{2}\pi$  too closely), and the asymmetry of the trajectories about the  $z$ -axis.

## III. ISOTROPIC INJECTION OF UNIFORM VELOCITY PARTICLES IN THE NEUTRAL PLANE

We now consider the following problem which simulates an application in solar physics:

A cloud of identical charged particles of given energy is injected at  $t = 0$  isotropically through the vertical hemisphere ( $2\pi$  steradians) at some point in the neutral plane of an exponential field configuration. What is the spatial density distribution of the particles after time  $t$ ?

For analytical reasons it is necessary to introduce simplifications. From the statistical standpoint we may legitimately consider only the distribution of the guiding centres rather than the particles themselves, so that equations (17) may be used to give the individual trajectories; further, we shall restrict the specification of the spatial distribution to the distributions,  $P(y)$  and  $P(z)$ , integrated over planes specified by given values of  $y$  and  $z$ . (The distribution in the  $x$ -plane is trivial since the guiding centres are constrained to the  $y$ - $z$  plane.) In the search for analytical solutions we have found it necessary to use approximate methods; our approximations yield results which are valid only for small and large values of  $kVt$  ( $kVt \lesssim 2$ ;  $kVt \gg 2$ ), but these limiting cases give an adequate description of the evolution of the phenomenon.

Now the probability,  $P_t(z) dz$ , of a particle lying between  $z$  and  $z + dz$  after time  $t$  is related to the probabilities,  $P(\theta_0) d\theta_0$  and  $P(\psi_0) d\psi_0$ , of particles injected with given values of  $\theta_0$  and  $\psi_0$  respectively by the expression

$$P_t(z) = \int_0^{\frac{1}{2}\pi} P(\psi_0)P(\theta_0)\frac{\partial\psi_0}{\partial z} d\theta_0, \quad (18)$$

where  $z(t)$  is given in terms of  $\psi_0$  and  $\theta_0$  through equation (17b). For hemispherical isotropic injection we have, ignoring constants of normalization,  $P(\theta_0) = \sin \theta_0$ ,  $P(\psi_0) = 1$ ; whence

$$P_t(z) = \int_0^{\frac{1}{2}\pi} \sin \theta_0 \frac{\partial\psi_0}{\partial z} d\theta_0. \quad (19a)$$

Similarly,

$$P_t(y) = \int_0^{\frac{1}{2}\pi} \sin \theta_0 \frac{\partial\psi_0}{\partial y} d\theta_0. \quad (19b)$$

Approximate solutions to equations (19a) and (19b) (substituting equations (17a) and (17b) respectively) are found in Appendix II for the limiting cases of small and large  $kVt$ ; these are plotted in Figures 5 and 6. The approximations for large  $kVt$  are independent of  $t$ .

Thus, the evolution of the height distribution ( $z$ -distribution) of a cloud of particles injected isotropically into the neutral plane with identical speeds  $V$  is illustrated in Figure 5. From these results we infer that the cloud of particles has at all times a steep leading edge which advances vertically with speed  $V$ . Behind the leading edge the great majority of the particles are contained within a quasi-rectangular pulse whose depth (in units of  $z$ ) increases from zero at time  $t = 0$  to  $(2/k\gamma_{\max.}) \ln 2 \sim 2/k$  when  $t \sim 4/kV$ . For larger values of  $t$  the pulse of particles advances vertically with speed  $V$  and without substantial change in density or depth, whilst the tail of the distribution (which always extends back to  $z = 0$ ), is progressively attenuated.

Figure 6, which relates to the evolution of the  $y$ -distribution, indicates that (like the tail of the  $z$ -distribution) the wings of the  $y$ -distribution are progressively attenuated as  $kVt$  increases to large values. Our approximations do not enable us to

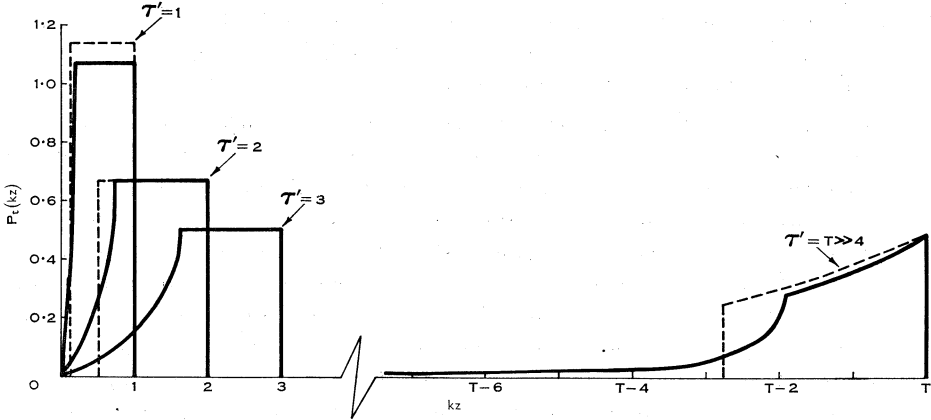


Fig. 5.—Height distributions (integrated over planes  $z = \text{constant}$ ) of a cloud of particles at times  $t$ . Injection occurs at  $t = 0$  with isotropic angular distribution over the vertical hemisphere and with identical speeds. The vertical magnetic field intensity varies as  $\exp(-kz)$ . The curves are labelled with values of  $\tau' = kVt$ . For details of the calculation of the curves see Appendix II. Full lines: injection into the neutral plane (Section III); broken lines: injection outside but near to the neutral plane (Section IV). Each set of distributions has been normalized to unit area under the curves.

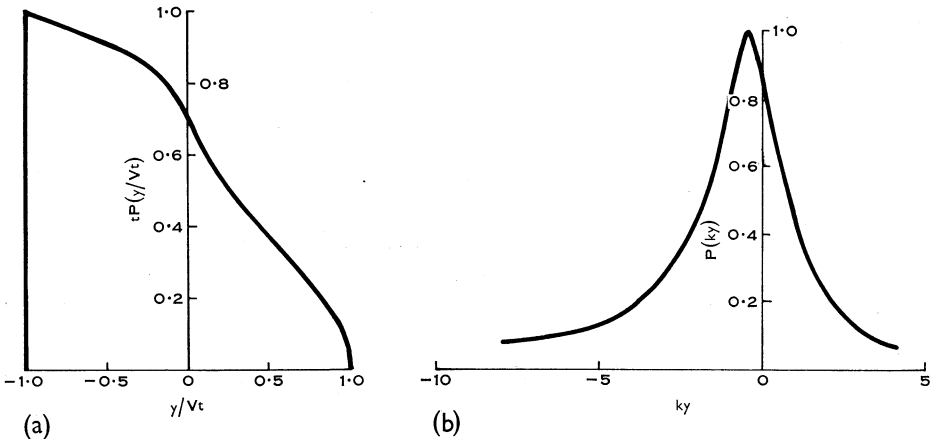


Fig. 6.— $y$ -distributions (integrated over planes  $y = \text{constant}$ ) for a cloud of particles injected into an exponential neutral plane. Injection conditions and notations are as in Figure 5. (a)  $t \approx 2/kV$ ; (b)  $t \gg 2/kV$ . The two curves have been normalized to  $P_{\text{max}} = 1$ .

follow the degradation of the steep leading edge initially present in the negative  $y$ -direction, but we presume that this will not persist beyond moderate values of  $kVt$ .

## IV. PARTICLES INJECTED OUTSIDE BUT NEAR TO THE NEUTRAL PLANE

The trajectories derived in Section II describe the motion of any particle that is able to reach the neutral plane, irrespective of the position at which injection occurs, but the particle density distributions of Section III apply only when the cloud is injected isotropically and exactly into the neutral plane as a point source. In practice, injection may well occur over a finite, though perhaps limited, area. In this case, the trajectories of the guiding centres of particles injected sufficiently close to the neutral plane may still be described approximately by equations (16) and (17), although the oscillatory motions about the guiding centres may be different because the particles do not necessarily cross the neutral plane. In particular, for injection at distances close to the neutral plane ( $x \ll 2(v_{\perp}/C)^{\frac{1}{2}}$ ) particles with azimuths  $\psi \rightarrow +90^\circ$  and  $\psi \rightarrow -90^\circ$  will drift in opposite directions along the neutral plane with approximately equal speeds ( $\sim V$ ). However, it is obvious from Figure 3 that for injection at greater distances ( $x \sim 2(v_{\perp}/C)^{\frac{1}{2}}$ ) the direction of drift is always in the positive  $y$ -direction, irrespective of the azimuth of injection, although the drift speed decreases from  $\sim V$  for  $\psi \rightarrow -90^\circ$  to  $\sim 0$  for  $\psi \rightarrow +90^\circ$ ; the direction of drift is also the same for injection on either side of the neutral plane. For injection at still larger distances from the neutral plane, that is,

$$x \gg 2(v_{\perp}/C)^{\frac{1}{2}}, \quad (20)$$

the  $y$ -drifts, which are evaluated in Appendix III, rapidly become negligible; the particles will then spiral along field lines with pitch angles decreasing with height in accordance with Alfvén's formula (8b).

Hence we see that there is a transition region, of half-width  $\sim 2(v_{\perp}/C)^{\frac{1}{2}}$ , in which the form of the trajectories changes smoothly from a complex three-dimensional oscillatory motion about a guiding centre constrained to the neutral plane to a helical motion along a field line. We shall not pause to detail the trajectories in this transition region but move out to the regions where the trajectories are essentially helical.\*

In this region the trajectory of a particle may be written (cf. equation (8b))

$$\sin^2\theta/\sin^2\theta_0 = B(s)/B(0), \quad (21)$$

where  $s$  denotes distance along the field line to which the particle is bound. Now the equation of a field line is obtained from

$$\frac{dx}{dz} = \frac{B_x}{B_z} = -\frac{1}{2}x \left\{ \frac{db(z)}{dz} / b(z) \right\}.$$

Hence, integrating,

$$x = x_0 \{b(z)/b(0)\}^{-\frac{1}{2}}, \quad (22)$$

where  $x_0$  denotes the value of  $x$  at injection ( $z = 0$ ). The value of  $B_z$  along a field line

\* A detailed discussion of trajectories in the transition region is given by Seymour (1959).

may thus be written\*

$$\begin{aligned} B_z(s) &= xb(s) = x_0\{b(s)b(0)\}^{\frac{1}{2}} \\ &= B_z(0)\{b(s)/b(0)\}^{\frac{1}{2}}. \end{aligned} \quad (23)$$

The total field is given by

$$B(s) = B_z(s) ds/dz = B_z(s)\{1+(dx/dz)^2\}^{\frac{1}{2}}.$$

For simplicity we restrict the discussion to regions of the field configuration where the inclination of the field lines to the vertical is small, that is,

$$(dx/dz)^2 \ll 1. \quad (24)$$

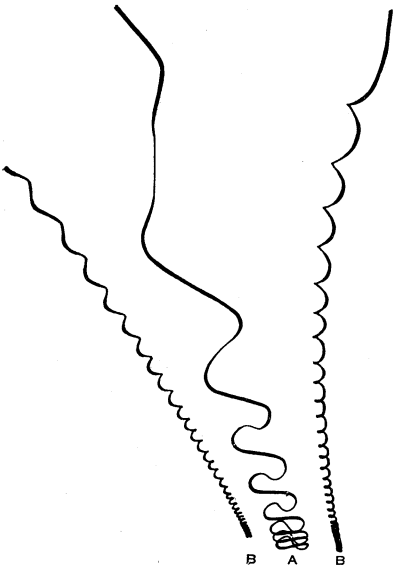


Fig. 7.—Illustrating, schematically but roughly to scale, the differences between trajectories of particles injected into, and near to, an exponential neutral plane. To relate the trajectories to a definite physical situation, we have taken the unit of distance as 1 solar radius,  $R_\odot$ . With this unit, the trajectories extend vertically over about  $1R_\odot$ , and the distance between the injection points for particles BB is  $\frac{1}{2}R_\odot$ .  $V/b(0) = 10^4 R_\odot^2/\text{gauss sec}$ , corresponding (if  $V \sim \frac{1}{3}c$ ) to a magnetic field intensity much weaker than those normally encountered in the lower corona (see Section VI). Particle A, which is injected horizontally ( $\theta_0 = \frac{1}{2}\pi$ ) into the neutral plane with azimuth angle  $\psi_0 \sim 40^\circ$ , loops vertically upwards. Particles BB, also injected horizontally, spiral in opposite senses up the field lines, which are almost vertical in the vicinity of the neutral plane.

The particle trajectory is then given by equations (21) and (23), thus

$$\sin^2\theta/\sin^2\theta_0 = \{b(s)/b(0)\}^{\frac{1}{2}}.$$

This is identical to (8a) if  $z$  is replaced by  $s$  and  $\gamma = \frac{1}{2}$ . This value of  $\gamma = \frac{1}{2}$  falls within the range of  $\gamma$  ( $0 \leq \gamma \leq 0.72$ ) which corresponds to arbitrary injection into the neutral plane. There will thus (Fig. 7) be a smooth transition between the vertical motion of the guiding centres in the neutral plane (described by (7)) and the motions along the field lines of the guiding centres for particles injected off the neutral plane, for which the equation of motion is

$$ds/dt = V[1-\{b(s)/b(0)\}^{\frac{1}{2}}\sin^2\theta_0]^{\frac{1}{2}}. \quad (25)$$

It should be stressed that this result is subject to the two conditions (20) and (24). With the aid of (1) and (22), recalling that  $C(z) = eb(z)/mc$ , the first of these

\* Equation (23) is a special case of a more general relation. If the vertical field intensity is taken as  $B_z = x^{2n+1}b(z)$ , it is easy to show that  $B_z(s) \sim B_z(0)\{b(s)/b(0)\}^{(2n+1)/(2n+2)}$ .

conditions reduces to

$$x_0 \gg 4v_{\perp}mc/eB_z(0), \quad (26)$$

i.e. the condition that, at injection, the local gyro radius must be small compared with the distance from the neutral plane. The second condition merely restricts the vertical inclination of the field lines.

(a) *Vertical Density Distributions for the Exponential Model*

Reverting now to the exponential model,  $b = b(0)e^{-kz}$  with  $s \equiv z$ , we find from (17b) that the integral of (25) is

$$z = (4/k)\ln\{\sin \theta_0 \cosh(\frac{1}{4}kVt - \ln \tan \frac{1}{2}\theta_0)\}. \quad (27)$$

The appropriate form of condition (24) is now  $k^2x^2 \ll 4$ .

The vertical density distributions  $P_t(z)$  (integrated over planes specified by given values of  $z$ ) for hemispherical isotropic injection of a cloud of identical charged particles can now be calculated in the same manner, and using the same approximations, as in Section III for the case of injection into the neutral plane. These distributions, which are derived in Appendix II(c), are independent of the injection coordinate  $x_0$ . They are sketched as broken lines in Figure 5.

We see, as indeed might have been anticipated from the similarity of the equations of motion in the two cases, that the distributions for injection points removed from the neutral plane are very similar to those for injection exactly into the neutral plane. The former distributions (injection off neutral plane) lack the tails of the latter (injection into neutral plane); this point of difference arises from the azimuth independence of the spiral trajectories. It is necessary to add, however, that the height distributions will remain insensitive to the size and location of the injection area only if the injection area does not extend too far from the neutral plane and injection is isotropic, or nearly so, in the angular variables. So long as these overall injection conditions are fulfilled the comparative independence of the height distributions on the location of the injection area is a convenient result, which relieves us of the necessity for a precise specification of the injection conditions in particular cases.

(b) *Radius of Gyration*

To complete our description of the motion of particles spiralling along field lines, we write down the formula for the gyro radius  $a$ . From (23), using  $v_{\perp}^2/v_{\parallel 0}^2 = B/B(0)$ , we find

$$a = \frac{1}{x_0} \left( \frac{mcV \sin \theta_0}{eb(0)} \right) e^{\frac{1}{2}kz}. \quad (28)$$

This should be compared with the  $x$ -loop dimension, derived from (9), for a particle injected into the neutral plane:

$$x_{\text{lim}} = \pm \{2(1 + \sin \psi_0)\}^{\frac{1}{2}} \left( \frac{mcV \sin \theta_0}{eb(0)} \right)^{\frac{1}{2}} e^{\frac{1}{2}kz(1-\frac{1}{2}\gamma)}. \quad (29)$$

The proportional rate of increase with height of the loop half-width (29) is always larger than that of the gyro radius (28).

## V. HEIGHT DEPENDENCE OF THE TEMPORAL DISTRIBUTION OF A CLOUD OF PARTICLES

As another aspect of our discussion of the density distributions we now seek the inverse of the  $z$ -distributions of Figure 5, and so derive the  $t$ -distributions at given  $z$ ,  $P_z(t)$ . The distributions we seek give the time dependence of the particle density (integrated over a plane specified by a given value of  $z$ ) in the cloud as it passes an observer situated at the given level  $z$ . From the preceding section we may anticipate that under the chosen injection conditions (hemispherical and isotropic) the  $t$ -distributions will not be sensitive to the location of the injection area and we confine the discussion to the simpler case of injection off the neutral plane. By inverting (56) and (58) (Appendix II) and evaluating  $P_z(t) = \sin \theta_0 d\theta_0/dt$  we obtain the limiting cases:

(a) for  $t \lesssim 2/kV$

$$\left. \begin{aligned} P(t) &\propto \{(\frac{1}{2}kVt)^2 - kz(\frac{1}{2}kVt - 2)\} / \{(\frac{1}{2}kVt)^2(4 - \frac{1}{2}kVt)^2\}, & z \leq Vt \leq 2\sqrt{2z}, \\ &= 0, & \text{elsewhere,} \end{aligned} \right\} \quad (30a)$$

(b) for  $t \gg 2/kV$

$$\left. \begin{aligned} P(t) &\propto \exp\{\frac{1}{4}k(z - Vt)\}, & z \leq Vt \leq z + (4/k)\ln 2, \\ &= 0, & \text{elsewhere.} \end{aligned} \right\} \quad (30b)$$

These density distributions, which illustrate the development with height of a cloud of particles injected simultaneously with identical speeds, are sketched in Figure 8(a), with  $k = 5$  (in units of  $z^{-1}$ ) and  $V = \frac{1}{8}$  (in units of  $z$  per second).

It is of interest to see how these time distributions are modified by the inclusion of time and velocity dispersions in the source function. Therefore in Figure 8 we show also the results of convoluting the distributions (30) with two separate dispersion functions, namely,

$$F(t) = \exp\{-(t-t_0)^2/2\sigma^2\} \quad \text{and} \quad F(V) = \exp\{-(V-V_0)^2/2\alpha^2\}.$$

Again  $k = 5$ ,  $V_0 = \frac{1}{8}$ ; and we have chosen  $\sigma = 1$  s,  $\alpha = 1/36$  (in units of  $z$  per second) so obtaining rise times with standard deviations  $\sim 1$  s at  $z = 1$  for both dispersion functions. For the purposes of the convolutions, the basic  $t$ -distribution at  $z = 1$  is represented with sufficient accuracy by the large  $t$ -distribution (58) (Appendix II). The temporal distributions of Figures 8(b) and 8(c) should apply without substantial modification to the case of injection into the neutral plane. They serve to indicate how time and velocity dispersions at the source are reflected in the density distribution of the cloud of particles as it moves upwards, and suggest that it should be possible to recover information on the properties of the source from a study of the changes in the form and peak density of the cloud as a function of height above the injection point.

## VI. APPLICATION TO TYPE III SOLAR RADIO BURSTS

In this section we examine the neutral plane configuration as a possible model for the source of a solar radio burst of spectral type III, and indicate the kinds of

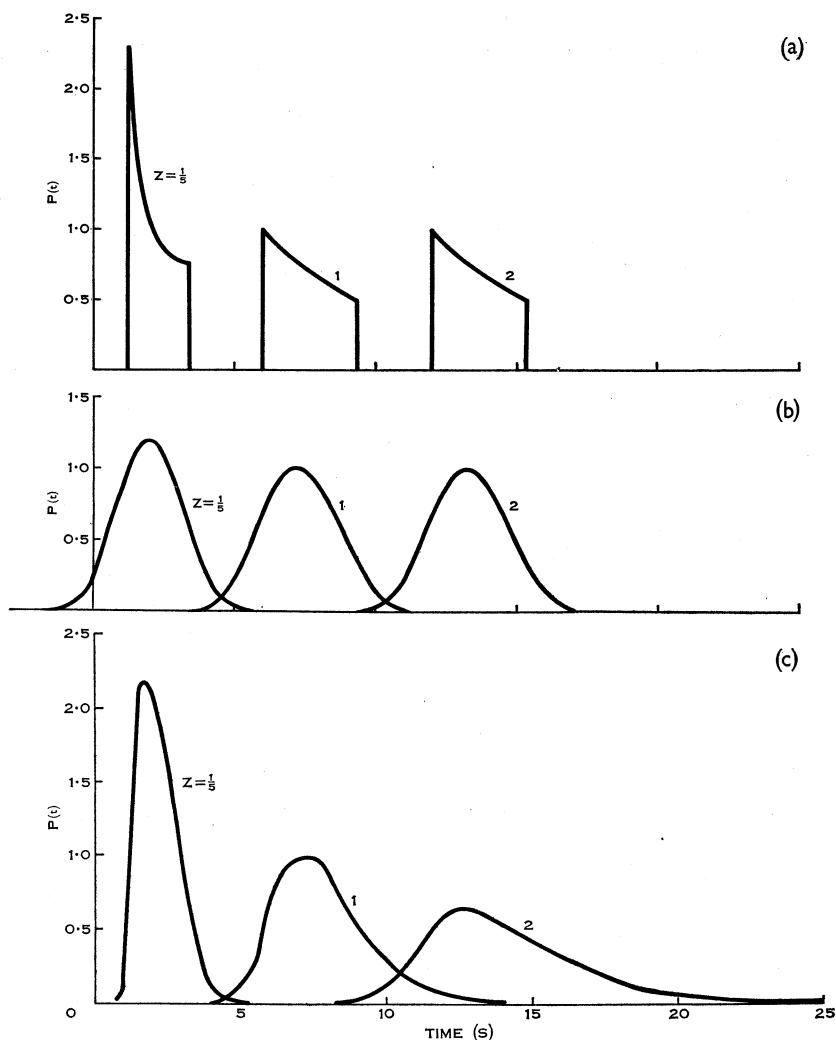


Fig. 8.—Illustrating the development with height  $z$  of the time distribution of a cloud of particles (integrated over planes  $z = \text{constant}$ ) moving up a neutral plane with vertical field gradient  $\exp(-5z)$ . The particles are injected isotropically over the vertical hemisphere at  $z = 0$ . The curves depict the time dependence of the particle density seen by observers at the heights indicated against the curves. (a) injection at  $t = 0$  with speed  $V = \frac{1}{5}$  (in units of  $z/s$ ); (b) injection with time dispersion  $F(t) = \exp(-\frac{1}{2}t^2)$  and uniform speeds  $V = \frac{1}{5}s$ ; (c) injection at  $t = 0$  with velocity dispersion  $F(V) = \exp\{-648(V - \frac{1}{5})^2\}$ . All three sets of curves are normalized to  $P_{\text{max}} = 1$  at  $z = 1$ . Assuming the intensity of radio emission to be proportional to the electron density, these distributions may correspond to time profiles of type III solar radio bursts measured at fixed frequencies.  $z = \frac{1}{5}$  corresponds to a frequency  $\sim 200$  Mc/s,  $z = 1$  to  $\sim 50$  Mc/s, and  $z = 2$  to  $\sim 20$  Mc/s. The dispersion parameters were chosen so that the distributions for  $z = 1$  are similar to the time profiles observed for type III bursts at 40 Mc/s by Weiss and Sheridan (1962).

data most suitable for the observational test of the validity of such a model. It will become apparent that the formulation of the preceding mathematical problems has been strongly influenced by this application.\*

We adopt the plasma hypothesis for the generation of type III emission. In its current specialized form this hypothesis supposes that the burst is produced by a sharp pulse of electrons (unaccompanied by protons) which is ejected from the vicinity of a flare, either low in the corona or near the top of the chromosphere. As the pulse of electrons moves out through regions of decreasing density, it excites plasma waves whose frequency decreases with time. This hypothesis predicts that decreasing frequencies of emission should originate from systematically increasing heights in the solar atmosphere, a prediction which has been substantiated by interferometer studies of Wild, Sheridan, and Neylan (1959). Type III bursts extend in frequency from  $\sim 400$  Mc/s to less than 5 Mc/s; the lower frequency limit (if any) is obscured by ionospheric cut-off. With a coronal density 10 times the Baumbach-Allen model, the corresponding heights range from  $4 \times 10^4$  km ( $0.05R_{\odot}$ ) to  $> 1.6 \times 10^6$  km ( $> 2R_{\odot}$ ) above the photosphere.

From the neutral plane model for the type III source we make two predictions which can be subjected to immediate observational test. Firstly, the pulse of electrons will have a steep leading edge which advances vertically with substantially constant speed  $V$ , equal to the injection speed of the electrons. The latter part of this prediction is confirmed by unpublished measurements by Stewart (in preparation), who finds that the leading edges of the sources of many individual type III bursts have essentially constant speeds over the height range  $0.3$  to  $2R_{\odot}$  above the photosphere. Observed speeds (Wild, Sheridan, and Neylan 1959; Hughes and Harkness 1963; and Stewart, in preparation) range from  $0.2$  to  $0.8c$  with a most probable speed between  $0.3$  and  $0.4c$ . We shall therefore take  $V = \frac{1}{3}R_{\odot}/s \sim 0.4c$  as a representative value for the injection speed.

Secondly, if, as seems probable, the injection of electrons into the neutral plane occurs over a finite though short interval of time and with not too great velocity dispersion, the particle density distributions illustrated in Figure 8 may describe one aspect of the development of a type III source. These distributions, which would extend over the frequency range from  $\sim 200$  Mc/s ( $z = \frac{1}{5}$ ) to  $\sim 20$  Mc/s ( $z = 2$ ), suggest that the intensity of type III emission, measured as a function of time at a given frequency, should show a rapid but not abrupt rise to a maximum value, followed by a slower decay. The distributions for  $z = 1$  in Figure 8(c) are in fact very similar to the intensity profiles† for some uncomplicated type III bursts at 40 Mc/s studied by Weiss and Sheridan (1962). This and other evidence (Elgaroy and Rodberg 1963;

\* In applying the foregoing theory to type III radio bursts we have ignored the interaction of the electron cloud with the background coronal plasma, electrostatic repulsions within the cloud, and electrostatic forces arising from charge separation at the time of acceleration in the flare region. Our application will be valid when the distance between the electrons in the cloud exceeds the Debye length for the surrounding coronal plasma. It is not clear how the behaviour of the electron cloud should be modified when the separation between the electrons is less than the Debye length.

† The time scale in Figure 4 of Weiss and Sheridan (1962) should be approximately halved to obtain an average true time scale.

Hughes and Harkness 1963) suggest that velocity dispersion may dominate over time dispersion at injection. We realize, of course, that direct comparison of Figure 8 with observed intensity profiles may be an oversimplification, as we ignore other factors which undoubtedly contribute to the shaping of the intensity profile observed at the Earth. For instance, collision damping of plasma waves in the corona (Westfold 1949; Wild 1950) is alone capable of explaining the observed exponential decay of the emission. Other factors requiring consideration are: (i) structure of the coronal density distribution near type III sources (perhaps in coronal streamers); (ii) natural bandwidth of excitation of plasma waves; (iii) dependence of emissive power of an electron on its velocity and pitch angle (which may profoundly modify the effects of velocity and angular dispersions); and (iv) group delays in propagation through the solar atmosphere. Nevertheless, we feel that the comparison made here is meaningful as a first approximation, and that the observed intensity profiles are consistent with the predictions of the neutral plane model.

The model leads to definite predictions concerning the brightness distributions of type III bursts. These may become subject to observational test as new techniques are developed, provided either that the brightness distributions as observed do not differ greatly, through refraction and scattering, from the true distributions, or that the necessary corrections can be applied. If injection occurs over a very small area centred on the neutral plane, the model suggests that the brightness distribution will lack circular symmetry, being narrow in the direction perpendicular to the neutral plane and elongated along it. As the injection area increases the source will enlarge laterally and tend to become more symmetrical. The source dimensions should increase monotonically with height. In making these predictions we rely on the reasonable assumption that the magnetic field intensity is large enough for the brightness distribution to be determined by the trajectories of the guiding centres and not by the amplitudes of the oscillatory motions about the guiding centres.

The existing sparse information on type III source dimensions, which has been obtained by strip scans with two-element interferometers and reduced on the assumption of Gaussian or other equally simple brightness distributions, is inadequate for testing these predictions. The material is collected in Figure 9. If, despite its limitations, we interpret these data as indicating the source size normal to the neutral plane, we obtain a value of  $k \sim 3$  (in units of  $R_{\odot}^{-1}$ ) and an average injection region with half-power half-width  $w \sim R_{\odot}/15$ . Since the effects of scattering are unknown, the derived injection area, which is little larger than the area of a large flare, must represent an upper limit.

If the above values of  $k$  and  $w$  are representative, the inequality  $k^2x^2 \ll 4$ , which is basic to much of the discussion of Sections IV and V, is valid for heights up to  $\sim 2R_{\odot}$ . But if the true value of  $k$  greatly exceeds  $3/R_{\odot}$  this inequality no longer holds and the treatment in Sections IV and V will not describe a type III source unless the injection area is comparatively small. It should also be recalled that in any case the model cannot apply at great heights in the solar atmosphere, where the pitch angle  $\theta$  becomes small and  $b(z)$  is no longer even approximately constant over a loop. Indeed, this second condition ( $b(z)$  approximately constant over a loop) may well prove to be more restrictive than the first ( $k^2x^2 \ll 4$ ). However, at great heights the magnetic field configuration may play a secondary role. Once a sufficiently large number of

electrons has been guided into vertical rectilinear motion the electron pulse will preserve its form, and particularly its sharp front, even in a field-free region. In view of the very low densities involved, the form of the cloud at great heights is more likely to be determined by the initial velocity dispersion than by other dispersive effects such as residual magnetic field, collisions, and self-diffusion.

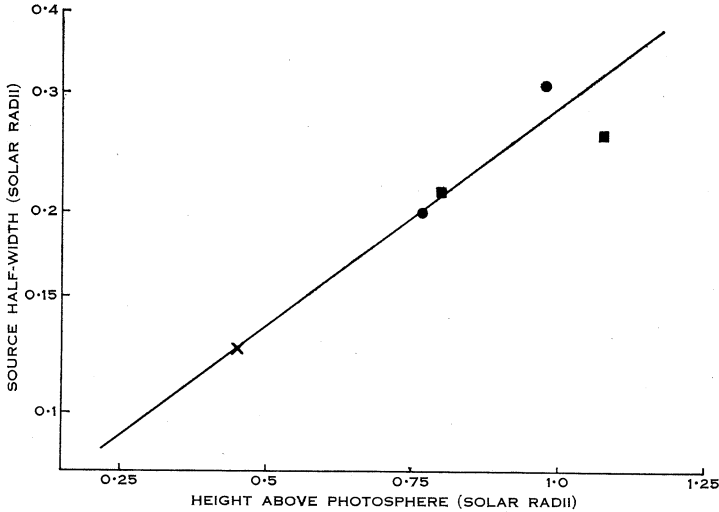


Fig. 9.—Half-widths of sources of type III solar radio bursts as a function of the height of the source above the photosphere.  $\times$  Goldstein (1959);  $\bullet$  Wild and Sheridan (1958);  $\blacksquare$  Weiss and Sheridan (1962). Frequencies have been converted to heights assuming an electron density  $10 \times$  Baumbach-Allen model. The full line shows the relation expected on the neutral plane model with  $k = 3/R_{\odot}$  and an injection radius of  $0.064R_{\odot}$  at the photosphere.

The assumption that the amplitudes of the oscillatory motions about the guiding centres are much smaller than the source dimensions cannot be verified without knowing the field intensity (or equivalently the transverse field gradient  $b$ ), and here we shall merely examine the plausibility of this assumption. We note from (22), (28), and (29) that the loop dimension  $x_{lim}$  and the gyro radius  $a$  both increase with height more slowly than  $x/x_0$  along a field line. It is therefore sufficient to examine the plausibility of the assumption at the injection level. From (28) the largest value of  $a$  (at  $\theta_0 = \frac{1}{2}\pi$ ) for given  $w$  is

$$a_{\max} \sim mcV/eb(0)w.$$

If we require

$$a_{\max}/w \ll 1, \quad (31)$$

then

$$b(0) \gg 5 \times 10^{-8}(V/w^2).$$

Putting  $V = \frac{1}{8}R_{\odot}/s$  and  $w = R_{\odot}/20$ , we get  $b(0) \gg 10^{-16}$  gauss/cm. For comparison we may take, as typical values for solar magnetic field gradients, the gradient within a large spot ( $\sim 10^{-6}$  gauss/cm) or that near a flare ( $> 5 \times 10^{-7}$  gauss/cm)

(Severny 1962). Also, combining the inequalities (20) and (24), which jointly determine the domain of applicability of the treatment in Sections IV and V, we obtain

$$2\{v_1 mc/eb(z)\}^{\frac{1}{2}} \ll 2/k. \quad (31a)$$

Substituting  $V = 10^{10}$  cm/s,  $b(0) = 10^{-6}$  gauss/cm and  $k = 3/R_{\odot}$ , we find that (31a) is satisfied by at least 5 orders of magnitude at  $z = 2R_{\odot}$  and by a still larger margin at  $z = 0$ . Even after allowing for distortion and compression of fields near the neutral plane, there is evidently little likelihood that the inequalities (31) and (31a) will be violated within a type III source.

Throughout this discussion of type III bursts we have taken the injection area as being centred, more or less, on the neutral plane. If we remove this restriction, and allow the injection area to be displaced to one side of the neutral plane, the pulse of electrons will be guided by the field lines away from the neutral plane. The resulting radio burst will then have a leading edge which appears curved on dynamic spectral records. In the extreme case when the field line returns to the low corona a "U" or "inverted J" burst could be generated. Accurate data on the relative positions of the two legs of U bursts would provide valuable information on this type of magnetic configuration. It would also be interesting to ascertain whether U bursts are relatively more frequent at times of high solar activity, when the development of re-entrant field lines may be facilitated by close approach of neighbouring active regions.

The type V burst (short-duration continuum emission following a type III burst) may be a further manifestation of injection away from the neutral plane; one may, for instance, suppose that such electrons are sometimes trapped within high magnetic loops to one side of the neutral plane, thus yielding the type V continuum. Since a type V burst is usually preceded by a type III burst with a straight spectral leading edge, the injection area for the composite III-V event may be supposed either large or composite, and the type V burst should commonly lie to one side of the type III burst, the combination forming a T-arrangement. There is indeed some evidence (Weiss and Stewart, in preparation) that the type V source is often displaced by a few minutes of arc from the position of the parent type III burst, but complete two-dimensional brightness distributions will be required for a satisfactory test of this hypothesis.

## VII. CONCLUSIONS

In this paper we have derived trajectories for individual particles, and density distributions for clouds of particles, injected into or near a neutral plane in a magnetic field, and with the aid of a simple field configuration we have indicated how the theory may provide a model for the source of a type III radio burst. We have shown that a cloud of particles of like charge injected within a limited volume, over a short time interval and with a small velocity dispersion, is formed by the magnetic field into a pulse with a steep leading edge which advances vertically with a speed equal to the injection speed of the particles. Such a steep leading edge and a constant speed are characteristic of the disturbances, taken to be brief compact pulses of electrons, which constitute type III radio sources. Even although the exponential model may not be an accurate description of the coronal field configurations, one may perhaps

infer more generally that the electron clouds will tend to delineate the shape of the guiding field, even when this is quite complex; and that the formation of a cloud of electrons into a sharp pulse with a steep leading edge will be characteristic of any magnetic field configuration whose intensity decreases with height.

Our knowledge of the strength and configuration of magnetic fields high in the corona is rudimentary. The ideas outlined in this paper suggest that the fast radio accompaniments of solar flares will prove to be a useful tool for the exploration of coronal magnetic fields and so help to fill this major gap in our knowledge of coronal structure—this in addition to giving information on the actual bursts of electrons emitted at the beginnings of flares.

On the theoretical side, there is still need to relate the observed spectral properties of type III bursts (which we take to include the associated type V bursts) to the characteristics of the burst sources. In Section VI we have indicated a possible approach to this problem, which should preferably be preceded by a more detailed examination of the role of the injection conditions (area, location relative to the neutral plane, and angular asymmetry) in determining the depth of the source. It is also desirable to extend the theory to include the effects of space charge and collisions, both of which may be important in the lower levels of the corona where the source is most compact and the ambient density is high. The theory also requires extension into the domain of relativistic electrons, since many type III sources have apparent speeds exceeding  $\frac{1}{2}c$ .

On the observational side, information on such injection parameters as time- and velocity-dispersion is undoubtedly latent in existing dynamic spectral records. For direct evidence on magnetic field configurations at the higher levels of the corona, two-dimensional brightness distributions, preferably measured at several frequencies for the same burst, appear to offer the most promise. However, the wanted data require instrumental techniques, for observing rapidly-varying brightness distributions, more sophisticated than the two-element interferometry that has hitherto been applied at metre wavelengths.

#### VIII. ACKNOWLEDGMENTS

The computations and drawings for this paper were ably performed by Miss Janet Rayner and Mr. D. W. Orchiston.

#### IX. REFERENCES

- BABCOCK, H. W. (1962).—*Trans. Int. Astr. Un.* **11B**: 419.  
 DELCROIX, J. L. (1960).—"Introduction to the Theory of Ionized Gases." p. 55. (Interscience Publishers: New York.)  
 DUNGEY, J. W. (1958).—I.A.U. Symposium No. 6, p. 135. (Cambridge Univ. Press.)  
 ELGARROY, O., and RODBERG, H. (1963).—*Nature* **199**: 268.  
 GOLD, T., and HOYLE, F. (1959).—*Mon. Not. R. Astr. Soc.* **120**: 89.  
 GOLDSTEIN, S. J. (1959).—*Astrophys. J.* **130**: 393.  
 HUGHES, M. P., and HARKNESS, R. L. (1963).—*Astrophys. J.* **138**: 239.  
 PARKER, E. N. (1963).—*Astrophys. J. (Suppl. 77)* **8**: 177.  
 PETSCHKE, H. (1963).—N.A.S.A.-A.A.S. Symposium on the Physics of Solar Flares, Greenbelt, Md., Oct. 1963.

SEVERNY, A. B. (1962).—*Trans. Int. Astr. Un.* **11B**: 426.  
 SEYMOUR, P. W. (1959).—*Aust. J. Phys.* **12**: 309.  
 SWEET, P. A. (1958).—I.A.U. Symposium No. 6, p. 123. (Cambridge Univ. Press.)  
 WEISS, A. A., and SHERIDAN, K. V. (1962).—*J. Phys. Soc. Japan (Suppl. A-II)* **17**: 223.  
 WESTFOLD, K. C. (1949).—*Aust. J. Sci. Res. A* **2**: 169.  
 WILD, J. P. (1950).—*Aust. J. Sci. Res. A* **3**: 541.  
 WILD, J. P., and SHERIDAN, K. V. (1958).—*Proc. Inst. Radio Engrs., N.Y.* **46**: 160.  
 WILD, J. P., SHERIDAN, K. V., and NEYLAN, A. A. (1959).—*Aust. J. Phys.* **12**: 369.

APPENDIX I

*Evaluation of  $\langle x^2 v_y \rangle_{b(z)}$  over a Loop*

By definition

$$\langle x^2 v_y \rangle_{b(z)} = \frac{\int x^2 (dy/dt) dt}{\int dt}. \tag{32}$$

Writing

$$dx/dt = v_{\perp} \cos \psi, \quad dy/dt = v_{\perp} \sin \psi, \tag{33}$$

equation (4) becomes

$$x^2 = (2v_{\perp}/C)(\sin \psi - \sin \psi_0),$$

whence

$$x dx/d\psi = -(v_{\perp}/C) \cos \psi. \tag{34}$$

Here, as before,  $C(z) = eb(z)/mc$ . From (32), (33), and (34) we have, as quoted in the text,

$$\langle x^2 v_y \rangle_{b(z)} = \frac{2v_{\perp}^2}{C(z)} \frac{I_2(\psi_0)}{I_1(\psi_0)} = -\frac{v_{\perp}^2 mc}{eb(z)} \gamma(\psi_0), \tag{5}$$

if  $\gamma = -2I_2(\psi_0)/I_1(\psi_0)$ . The integrals  $I_1$  and  $I_2$  are respectively

$$I_1(\psi_0) = \int_{\psi_0}^{-\frac{1}{2}\pi} (\sin \psi_0 - \sin \psi)^{-\frac{1}{2}} d\psi,$$

$$I_2(\psi_0) = \int_{\psi_0}^{-\frac{1}{2}\pi} \sin \psi (\sin \psi_0 - \sin \psi)^{\frac{1}{2}} d\psi.$$

The limits in each case correspond to integration over a quarter-loop. We note that  $I_1$  is related to  $T$ , the time required for the particle to traverse a quarter-loop, through the relation

$$I_1 = (2Cv_{\perp})^{\frac{1}{2}} T. \tag{35}$$

By means of the substitutions

$$-2\phi = \psi + \frac{1}{2}\pi, \quad \sin u = \sin \phi / \sin \phi_0, \tag{36}$$

the integral  $I_1$  transforms to

$$I_1 = 2^{\frac{1}{2}} \int_0^{\frac{1}{2}\pi} \{1 - \sin^2(\frac{1}{2}\psi_0 + \frac{1}{4}\pi) \sin^2 u\}^{-\frac{1}{2}} du$$

$$= 2^{\frac{1}{2}} K.$$

and we obtain

$$T = (Cv_1)^{-\frac{1}{2}}K, \quad (14)$$

which is identical with (14), which was derived in the text using a different system of variables. As before,  $K = K\{\sin(\frac{1}{2}\psi_0 + \frac{1}{4}\pi)\}$ .

Again using the substitution (36) we find that  $I_2$  may be written as

$$I_2 = -2^{3/2} \int_0^{\frac{1}{2}\pi} \frac{(1-2\sin^2\phi_0\sin^2u)\sin^2\phi_0\cos^2u}{(1-\sin^2\phi_0\sin^2u)^{\frac{3}{2}}} du.$$

Using the standard reductions for  $\int \sin^nu(1-\sin^2\phi_0\sin^2u)^{-\frac{1}{2}} du$  and

$$\int \cos^nu(1-\sin^2\phi_0\sin^2u)^{-\frac{1}{2}} du,$$

we finally obtain

$$\begin{aligned} I_2 &= -(2^{3/2}/3)\{(1-2\cos^2\phi_0)E + \cos^2\phi_0 \cdot K\} \\ &= -(2^{\frac{3}{2}}/3)\{2E\sin\psi_0 + K(1-\sin\psi_0)\}, \end{aligned}$$

and hence

$$\gamma(\psi_0) = -2I_2/I_1 = \frac{2}{3}\{1 + (2E/K - 1)\sin\psi_0\}, \quad (6)$$

as quoted in the text.

## APPENDIX II

### *Approximations for the Spatial Distributions of a Cloud of Particles Injected Isotropically into or near a Neutral Plane*

For the purpose of evaluating the spatial density distributions we shall replace the time  $t$  and the spatial variables  $y$  and  $z$  by the dimensionless system

$$\tau = \frac{1}{2}kVt, \quad \eta = ky, \quad \zeta = kz.$$

In terms of these dimensionless variables, we rewrite (17a) and (17b) as

$$\eta = -\frac{4}{\sin\psi_0} \left( \frac{3}{2} - \frac{1}{\gamma} \right) \{ \arctan(e^{\gamma\tau} \cot \frac{1}{2}\theta_0) - \frac{1}{2}(\pi - \theta_0) \}, \quad (37)$$

$$\zeta = (2/\gamma) \ln \{ \sin\theta_0 \cosh[\gamma\tau - \ln \tan \frac{1}{2}\theta_0] \}. \quad (38)$$

(a)  *$\zeta$ -Distributions for Injection into Neutral Plane.*—The  $\zeta$ -distributions are most conveniently evaluated by changing to a system of axes advancing vertically with speed  $V$ , i.e. to a system co-moving with the leading edge of the cloud of electrons. In this axis system the probability equation (19a) for hemispherical isotropic injection becomes

$$P_\tau(2\tau - \zeta) = - \int_0^{\frac{1}{2}\pi} \sin\theta_0 \frac{\partial\gamma}{\partial\zeta} \frac{d\psi_0}{d\gamma} d\theta_0, \quad (39)$$

if we also substitute  $(\partial\gamma/\partial\zeta)(d\psi_0/d\gamma)$  for  $\partial\psi_0/\partial\zeta$  (since  $\gamma$  is a function of  $\psi_0$  only,  $\partial\psi_0/\partial\gamma \equiv d\psi_0/d\gamma$ ). The form of  $d\psi_0/d\gamma$  obtained from (6) can be simplified by the parabolic approximation

$$\gamma = \gamma_m - \text{const.}(\psi_0 - \psi'_0)^2. \tag{40}$$

$\gamma_m = 0.72$  is the maximum value of  $\gamma$ . Although  $\gamma$  is not symmetrical about  $\psi'_0 \sim 20^\circ$ , the error in this approximation is reduced by the circumstance that in evaluating (39) we must average  $d\psi_0/d\gamma$  over both halves of the  $(\gamma, \psi_0)$  curve. After averaging, the error in  $d\psi_0/d\gamma$  is less than 15% for  $\gamma > 0.1$ ; it increases rapidly as  $\gamma \rightarrow 0$  for negative  $\psi_0$  (i.e.  $\psi_0 < -60^\circ$ ), but the error will be important only in the tail of the  $\zeta$ -distribution.

(i) *Small  $\tau$  approximation* ( $\tau \lesssim 1.5$ ).—Consideration of (38) under the three limiting conditions: (a)  $\theta_0 = \frac{1}{2}\pi$ ,  $\tau \rightarrow 0$ ; (b)  $\gamma = 0$ , all  $\tau$ ; and (c)  $\theta_0 = 0$ , all  $\tau$ , suggests that for small  $\tau$  we may approximate (38) by

$$\zeta = 2\tau \cos \theta_0 + \gamma\tau^2(1 - \cos \theta_0),$$

that is,

$$2\tau - \zeta = 2(2\tau - \gamma\tau^2)\sin^2\frac{1}{2}\theta_0. \tag{41}$$

The error in this approximation has been examined by numerical sampling and is less than 5% for  $\tau \leq 1.5$  except when  $\theta_0 > 80^\circ$  and  $\tau \sim 1.5$ . Differentiating (40) and (41) and substituting into (39) gives, apart from an omitted constant,

$$P(2\tau - \zeta) = \frac{2^{\frac{1}{2}}}{\tau(2\tau - \zeta)^{\frac{1}{2}}} \int_{\theta_1}^{\theta_2} \frac{\cos \frac{1}{2}\theta_0 \, d\theta_0}{[1 - \beta^2 \sin^2 \frac{1}{2}\theta_0]^{\frac{1}{2}}}, \tag{42}$$

where  $\beta^2 = 2(2\tau - \gamma_m\tau^2)/(2\tau - \zeta)$ . For the limits of integration,  $\theta_1 = \arccos(\zeta/2\tau)$ ;  $\theta_2 = \frac{1}{2}\pi$  for  $0 \leq \zeta \leq \gamma_m\tau^2$  and  $\theta_2 = 2 \arcsin(1/\beta)$  for  $\gamma_m\tau^2 \leq \zeta \leq 2\tau$ . The right-hand side of (42) can be integrated analytically to give

$$\begin{aligned} P(2\tau - \zeta) &= \frac{2}{\tau(2\tau - \gamma_m\tau^2)^{\frac{1}{2}}} \left[ \arcsin\left(\frac{2\tau - \gamma_m\tau^2}{2\tau - \zeta}\right)^{\frac{1}{2}} - \arcsin\left(\frac{2\tau - \gamma_m\tau^2}{2\tau}\right)^{\frac{1}{2}} \right], & 0 \leq \zeta \leq \gamma_m\tau^2, \\ &= \frac{2}{\tau(2\tau - \gamma_m\tau^2)^{\frac{1}{2}}} \left[ \frac{1}{2}\pi - \arcsin\left(\frac{2\tau - \gamma_m\tau^2}{2\tau}\right)^{\frac{1}{2}} \right], & \gamma_m\tau^2 \leq \zeta \leq 2\tau, \\ &= 0, & \zeta > 2\tau. \end{aligned} \tag{43}$$

(ii) *Large  $\tau$  approximation* ( $\tau \gg 2$ ).—For large values of the argument,  $\cosh u \sim \frac{1}{2}e^u$ . Hence for  $\tau > 2$ , (38) may be approximated by

$$2\tau - \zeta = -(4/\gamma)\ln \cos \frac{1}{2}\theta_0, \tag{44}$$

except in the tail of the  $\zeta$ -distribution where  $\gamma \rightarrow 0$  and  $\theta_0 \rightarrow \frac{1}{2}\pi$  simultaneously. Again differentiating (40) (omitting the constant) and (44) and substituting into (39), we obtain

$$P(2\tau - \zeta) = - \frac{2}{(2\tau - \zeta)^{3/2}} \int_0^{\theta_2} \frac{\ln \cos \frac{1}{2}\theta_0 \sin \theta_0 \, d\theta_0}{[\frac{1}{4}\gamma_m(2\tau - \zeta) + \ln \cos \frac{1}{2}\theta_0]^{\frac{1}{2}}} \tag{45}$$

in which

$$\begin{aligned} \theta_2 &= 2 \arccos[\exp\{-\frac{1}{4}\gamma_m(2\tau - \zeta)\}], & 2\tau - (2/\gamma_m)\ln 2 \leq \zeta \leq 2\tau, \\ &= \frac{1}{2}\pi, & 0 \leq \zeta \leq 2\tau - (2/\gamma_m)\ln 2. \end{aligned}$$

It is easy to show that as  $\theta_0 \rightarrow 0$ , i.e. as  $\zeta \rightarrow 2\tau$ , (45) tends to the value  $P(0) = (4/3)\gamma_m^{3/2} = 0.81$ . For other values of  $\zeta$ , the singularity in (45) at  $\theta_0 = \theta_2$  can be eliminated by means of the substitution  $\ln \cos \frac{1}{2}\theta_0 = u^2 - \frac{1}{4}\gamma_m(2\tau - \zeta)$ . We obtain

$$P(2\tau - \zeta) = \frac{16}{(2\tau - \zeta)^{3/2}} \int_{u_1}^{u_2} \{u^2 - \frac{1}{4}\gamma_m(2\tau - \zeta)\} \exp[2\{u^2 - \frac{1}{4}\gamma_m(2\tau - \zeta)\}] du, \quad (46)$$

$$u_1 = \frac{1}{2}\{\gamma_m(2\tau - \zeta)\}^{\frac{1}{2}},$$

$$u_2 = 0, \quad 2\tau - (2/\gamma_m)\ln 2 \leq \zeta \leq 2\tau,$$

$$= \frac{1}{2}\{\gamma_m(2\tau - \zeta) - 2 \ln 2\}^{\frac{1}{2}}, \quad 0 \leq \zeta \leq 2\tau - (2/\gamma_m)\ln 2.$$

The integral in (46) has been evaluated by standard numerical methods.

(b)  *$\eta$ -Distributions for Injection into the Neutral Plane.*—The appropriate form for the probability integral (cf. equation (19b)) is now

$$P_\tau(\eta) = \int_0^{\frac{1}{2}\pi} \sin \theta_0 \frac{\partial \psi_0}{\partial \eta} d\theta_0. \quad (47)$$

(i) *Small  $\tau$  approximation* ( $\tau \lesssim 1$ ).—When  $\theta_0 = \frac{1}{2}\pi$ , (37) reduces to  $\eta = F(\psi_0)gd(\gamma\tau)$ , where we have written

$$F(\psi_0) = -\frac{2}{\sin \psi_0} \left( \frac{3}{2} - \frac{1}{\gamma} \right),$$

and

$$gd u = \text{Gudermannian } u = \int_0^u \frac{dt}{\cosh t} = 2 \arctan e^u - \frac{1}{2}\pi.$$

From the expansion  $gd u = u - u^3/6 + u^5/24 + \dots$ , we have, with an error  $< 10\%$  when  $\tau < 1$  and  $\theta_0 = \frac{1}{2}\pi$ ,

$$\eta \sim \gamma F(\psi_0)\tau. \quad (48)$$

Also, when  $\gamma\tau$  is small but  $\cot \frac{1}{2}\theta_0$  is large, i.e. as  $\theta_0 \rightarrow 0$ , we may use the asymptotic expansion  $\arctan u = \frac{1}{2}\pi - 1/u + 1/3u^3 \dots$  to obtain

$$\eta \sim \gamma F(\psi_0)\tau \theta_0 \sim \gamma F(\psi_0)\tau \sin \theta_0. \quad (49)$$

The replacement of  $\theta_0$  by  $\sin \theta_0$  in (49) is suggested by the form of (48) for  $\theta_0 = \frac{1}{2}\pi$  and by noting that when  $\gamma = 0$ ,  $\eta = \pm 2\tau \sin \theta_0$  for all  $\theta_0$ . Hence we shall adopt (49) as the small  $\tau$  approximation for  $\eta$ , valid when  $\tau \lesssim 1$ ; it is accurate to within 25% except perhaps when  $\theta_0 \sim \frac{1}{4}\pi$ . The form of (49) is, however, not suitable for evaluating  $\partial \psi_0 / \partial \eta$ , and so we make the further approximation

$$\gamma F(\psi_0) = \frac{4}{\pi} \left\{ \psi_0 + \frac{1}{\pi} (\psi_0^2 - \frac{1}{4}\pi^2) \right\},$$

which, to the accuracy we seek, is a good representation of the function  $\gamma F(\psi_0)$ . The probability integral (47) can now be evaluated; we find

$$2\tau P(\eta) = \frac{\pi}{2^{3/2}} \int_{\theta_1}^{\frac{1}{2}\pi} \left\{ 1 + \frac{\eta}{2\tau \sin \theta_0} \right\}^{-\frac{1}{2}} d\theta_0, \quad (50)$$

where  $\theta_1 = \arcsin|\eta/2\tau|$ . The errors involved in the use of (50) are not precisely known, but we are confident that (50) reproduces the significant features of the  $\eta$ -distribution for small values of  $\tau$  ( $\tau \lesssim 1$ ).

Numerical evaluation of (50) is straightforward only if  $\eta \geq 0$ . For  $\eta = 0$  the integral has the value  $\frac{1}{2}\pi$ . When  $\eta < 0$  the integrand diverges at  $\theta_0 = \theta_1$ , and (50) has been evaluated by terminating the numerical integration at  $|\eta/2\tau| + \delta$ , and approximating the integral over the small remaining interval  $\delta$  by

$$I = \frac{1}{(1-u^2)^{\frac{1}{2}}} \int_u^{u+\delta} \{\sin \theta_0 / (\sin \theta_0 - u)\}^{\frac{1}{2}} d(\sin \theta_0),$$

( $u = |\eta/2\tau|$ ) which can be integrated analytically. For  $\eta < -0.8$ , a better approximation to the integral is given by

$$\begin{aligned} I &\sim (\sin \theta_1)^{\frac{1}{2}} \int_{\theta_1}^{\frac{1}{2}\pi} (\sin \theta_0 - \sin \theta_1)^{\frac{1}{2}} d\theta_0 \\ &= (2|\eta/2\tau|)^{\frac{1}{2}} K \sin \frac{1}{4}(\pi - 2\theta_1). \end{aligned}$$

(ii) *Large  $\tau$  approximation* ( $\tau \gg 1$ ).—When  $\tau \gg 1$ ,  $e^{\gamma\tau} \cot \frac{1}{2}\theta_0 \rightarrow \infty$  for all  $\theta_0$ , and we get the simple approximation

$$\eta \sim \theta F(\psi_0). \tag{51}$$

Inverting the roles of  $\psi_0$  and  $\theta_0$  in (47), this leads directly to

$$\begin{aligned} P(\eta) &= \int_{\alpha_1}^{\alpha_2} \sin \left\{ \frac{\eta}{F(\psi_0)} \right\} \frac{d\psi_0}{F(\psi_0)}, \\ F(\psi_0) &= -\frac{2}{\sin \psi_0} \left( \frac{3}{2} - \frac{1}{\gamma} \right). \end{aligned} \tag{52}$$

$\alpha_1$  is the solution of  $F(\alpha_1) = 2\eta/\pi$ ,  $\alpha_2 = \pm \frac{1}{2}\pi$ , when  $\eta \geq 0$ .

Expression (52) has been integrated numerically.

(c)  *$\zeta$ -Distributions for Injection Near the Neutral Plane.*—In this case, since the trajectories of the guiding centres are independent of the azimuth angle  $\psi_0$ , the probability equation (corresponding to (39)) for isotropic hemispherical injection is simply

$$P_\tau(\zeta) = \sin \theta_0 d\theta_0/d\zeta. \tag{53}$$

We now evaluate (53) in the small and large  $\tau$  approximations by rewriting equation (27) in terms of the dimensionless variables  $\tau$  and  $\zeta$ ,

$$\zeta = 4 \ln \{ \sin \theta_0 \cosh(\frac{1}{2}\tau - \ln \tan \frac{1}{2}\theta_0) \}. \tag{54}$$

(i) *Small  $\tau$  approximation* ( $\tau \lesssim 2$ ).—The small  $\tau$  approximation (compare (41)) is

$$\zeta = 2\tau \cos \theta_0 + \frac{1}{2}\tau^2(1 - \cos \theta_0), \tag{55}$$

which leads to

$$\begin{aligned} P(\zeta) &= (2\tau - \frac{1}{2}\tau^2)^{-1}, & \frac{1}{2}\tau^2 \leq \zeta \leq 2\tau, \\ &= 0, & \text{elsewhere.} \end{aligned} \tag{56}$$

(ii) *Large  $\tau$  approximation* ( $\tau \gg 2$ ).—We obtain from (44)

$$\zeta = 2\tau + 8 \ln \cos \frac{1}{2}\theta_0, \quad (57)$$

whence

$$P(\zeta) = \frac{1}{2} \exp -\left(\frac{2\tau - \zeta}{4}\right), \quad 2\tau - 4 \ln 2 \leq \zeta \leq 2\tau, \\ = 0, \quad \text{elsewhere.} \quad (58)$$

The density distributions (56) and (58) are plotted in Figure 5 as broken lines.

### APPENDIX III

#### *Transverse Drift of Particles Spiralling along Field Lines*

In regions where the particles can be regarded as spiralling along field lines, the transverse drift in the  $y$ -direction is given by

$$v_y = (mc/eBR)(v_{\parallel}^2 + \frac{1}{2}v_{\perp}^2) \quad (59)$$

(e.g. Delcroix 1960), where  $R$  is the radius of curvature of the field line.

For the exponential model, and in regions where  $k^2x^2 \ll 4$ , we have, using (22)

$$R \sim (4/kx_0)e^{-\frac{1}{2}kz}.$$

Also, if  $\theta$  is the pitch angle relative to the field line,

$$v_{\parallel}^2 + \frac{1}{2}v_{\perp}^2 = \frac{1}{2}V^2(2 - \sin^2\theta).$$

These last two expressions and equation (23) for  $B$ , when substituted into (59), give

$$v_y \sim \frac{1}{8} \left( \frac{mck^2V^2}{eb(0)} \right) e^{kz} (2 - \sin^2\theta). \quad (60)$$

Inserting the numerical values established in Section VI, i.e.  $V \sim 10^{10}$  cm/s,  $k \sim 3/R_{\odot}$ ,  $b(0) \sim 10^{-6}$  gauss/cm, we obtain  $v_y \sim 10^{-3}$  cm/s at  $z = 0$ . Even although the transverse drift may increase by several orders of magnitude over the range of heights traversed by the typical type III disturbance, the radius of curvature of the field lines in the vicinity of the neutral plane is so large that the transverse drift is at all times negligible in comparison with the vertical speeds.